The measured dependence of the lateral ambipolar diffusion length on carrier injection-level in Stranski-Krastanov quantum dot devices

D. Naidu, P. M. Smowton, and H. D. Summers

Citation: J. Appl. Phys. 108, 043108 (2010); doi: 10.1063/1.3471812
View online: http://dx.doi.org/10.1063/1.3471812
View Table of Contents: http://jap.aip.org/resource/1/JAPIAU/v108/i4
Published by the American Institute of Physics.

Related Articles

Electroluminescence from strained germanium membranes and implications for an efficient Si-compatible laser
Appl. Phys. Lett. 100, 131112 (2012)

A weakly coupled semiconductor superlattice as a potential for a radio frequency modulated terahertz light emitter
Appl. Phys. Lett. 100, 131104 (2012)

Quantum-dot nano-cavity lasers with Purcell-enhanced stimulated emission
Appl. Phys. Lett. 100, 131107 (2012)

Effect of internal optical loss on the modulation bandwidth of a quantum dot laser
Appl. Phys. Lett. 100, 131106 (2012)

Design of three-well indirect pumping terahertz quantum cascade lasers for high optical gain based on nonequilibrium Green's function analysis
Appl. Phys. Lett. 100, 122110 (2012)

Additional information on J. Appl. Phys.

Journal Homepage: http://jap.aip.org/
Journal Information: http://jap.aip.org/about/about_the_journal
Top downloads: http://jap.aip.org/features/most_downloaded
Information for Authors: http://jap.aip.org/authors

ADVERTISEMENT

Downloaded 02 Apr 2012 to 131.251.133.28. Redistribution subject to AIP license or copyright; see http://jap.aip.org/about/rights_and_permissions

The measured dependence of the lateral ambipolar diffusion length on carrier injection-level in Stranski-Krastanov quantum dot devices

D. Naidu, P. M. Smowton,[a] and H. D. Summers[b]
School of Physics and Astronomy, Cardiff University, Cardiff, CF24 3AA, United Kingdom

(Received 22 April 2010; accepted 30 June 2010; published online 26 August 2010)

Using the segmented contact method we separate and numerically evaluate the components making up the threshold current density dependence of quantum dot ridge waveguide lasers. An increasing internal optical mode loss and an increasing lateral out-diffusion current are the significant processes in ridges of widths between 4 and 10 μm, with no significant contribution from a deteriorating gain-mode overlap. By fitting a diffusion length model to the lateral out-diffusion process, we extract the ambipolar diffusion length, L_d, as a function of intrinsic carrier injection-level which covers carrier densities appropriate for functioning light-emitting diode and laser devices. The measured dependence fits a diffusion mechanism involving the thermal redistribution of carriers via the wetting-layer and most significantly leads to two regimes where L_d can be reduced in self-assembled quantum-dot systems. Only one of these is shown to be beneficial to the overall efficiency of the device, while the other is at the expense of undesired high-order nonradiative recombination processes at high injection-levels. Covering a peak modal gain range of approximately 5 to 11 cm^{-1} over injection-levels of 65 to 122 meV at 350 K, this dependence caused L_d to change from 0.75 to 1.50 μm, with the maximum occurring at 84 meV where the peak modal gain is 6 cm^{-1}. Decreasing the temperature to 300 K reduced L_d to <0.75 μm over approximately the same injection-level range. © *2010 American Institute of Physics*. [doi:10.1063/1.3471812]

I. INTRODUCTION

As semiconductor laser devices progressively reduce in size and involve etching through the active region for needs such as micro cavities and the integration of deep-etched photonic features, carrier diffusion in the plane of the active region plays an increasingly major role on the overall performance and efficiency. The "lateral" diffusion of carriers can lead to a spreading of the injected current to regions outside of where round-trip amplification occurs (lateral out-diffusion). It can also lead to nonradiative recombination by diffusion to surface-states at the etched sidewalls. The reduction in lateral diffusion is thus considered necessary.

Self-assembled quantum-dots have been successfully employed as the active region in semiconductor lasers and amplifiers[1,2] and are anticipated to prevent lateral diffusion by localizing carriers in all three dimensions.[3] In the literature, empirical studies have reported a reduction in lateral diffusion with quantum-dot active regions as compared to quantum-wells based on improvements in device performance.[4,5] Some have even attempted to compare the lateral ambipolar diffusion length (L_d) and shown it to be smaller in quantum-dots than quantum wells.[6–8] However, the values for L_d range considerably (0.1–5 μm) and more significantly there still remains some ambiguity in the mechanism of lateral diffusion in the coupled system of quantum-dots, wetting-layer, and barrier material.

To resolve this ambiguity, we perform an investigation of the lateral ambipolar diffusion length as a function of intrinsic carrier injection-level and temperature. The approach we use to measure L_d is in line with those which fit the threshold current density dependence on ridge width with a standard ambipolar diffusion length model.[8–10] However we use the segmented contact method[11] (SCM) to characterize the threshold behavior and by doing so improve and extend the overall analysis. Namely, we directly measure material characteristics such as the gain and recombination mechanisms rather than relying on specific laser models and additional sets of assumptions. We also evaluate the relative impact on the threshold dependence from the contributory mechanisms of an increasing internal optical loss,[12,13] deteriorating gain-mode overlap,[14–16] and increasing fraction of lateral out-diffusion.[9,10,17,18] This makes for a more correct estimate of L_d since the diffusion model is applied to the threshold dependence from lateral out-diffusion only. In the conventional approach these other mechanisms are difficult to account for experimentally with just laser threshold measurements, while further modeling and assumptions just adds to the complexity. Most significantly, with the SCM we can further the overall analysis by measuring the properties as a function of intrinsic carrier injection-level rather than being restricted to a single operating point. The range of carrier injection-levels that we perform the analysis on extends to the high injection-level regime where real "working" devices operate. In comparison, the cathodoluminescence[19,20] and photoluminescence[6,21,22] studies are performed under low injection-levels on specifically designed and sometimes unrealistic material structures.

With the SCM approach, we report that the mechanism

[a]Electronic mail: smowtonpm@cf.ac.uk.
[b]Present address: School of Engineering, Swansea University, Singleton Park, Swansea, SA2 8PP, United Kingdom.

 © 2010 American Institute of Physics

Downloaded 02 Apr 2012 to 131.251.133.28. Redistribution subject to AIP license or copyright; see http://jap.aip.org/about/rights_and_permissions

of lateral diffusion in the self-assembled quantum-dot system is strongly dependent on the level of carrier injection and temperature. The process is described by the thermal redistribution of carriers via the wetting-layer, and significantly results in two distinct regimes where the apparent lateral ambipolar diffusion length is reduced. Through measurements of the spontaneous emission, nonradiative current density, and overall internal quantum efficiency, we show that only one of these regimes is beneficial to overall device performance. The other is a reduction from undesired higher order nonradiative recombination processes. Together these observations allow us to stipulate the criteria for further improvements in device miniaturization and integration with quantum-dot active regions.

The paper begins, in Sec. II, by describing the sample structures used. In Sec. III we first evaluate the threshold current density dependence on ridge width. This is followed by a detailed characterization of the gain, internal optical loss, and recombination currents in each different ridge width. Through this we evaluate the relative contribution to the threshold increase from an increasing internal optical loss, deteriorating gain-mode overlap, and increasing lateral carrier out-diffusion loss. In Sec. IV, we fit the threshold dependence arising from lateral out-diffusion with a standard diffusion length model to determine L_d. Subsequently we analyze L_d as a function of intrinsic carrier injection-level and interpret the results.

II. EXPERIMENTAL

The quantum dot (QD) material used in this investigation has been optimized for 1.3 μm operation and was grown by solid source molecular beam epitaxy. The active region consisted of five Dot-in-a-Well (DWELL) repeats, where each DWELL consisted of 3.0 monolayers of InAs dots grown on 2 nm of $In_{0.15}Ga_{0.85}As$, capped with 6 nm of $In_{0.15}Ga_{0.85}As$. Each DWELL layer was separated by 50 nm GaAs high growth temperature spacer layers (HGTSLs). The GaAs spacer is initially grown at 510 °C for the first 15 nm, and then at 620 °C for the remaining 35 nm. Atomic force microscopy measurements on uncapped samples grown using similar conditions reveal a QD density of $\sim 4 \times 10^{10}$ cm^{-2}.[23] The use of HGTSLs has been shown to inhibit the formation of defects and dislocations in multilayer samples[24] and to result in low threshold current density devices.[23] The active region was incorporated into a $GaAs-Al_{0.4}Ga_{0.6}As$ waveguide structure.

The QD material was fabricated into multisection shallow-etch ridge devices of widths ranging from 4 to 10 μm with 300 μm long sections in a single fabrication process. The ridges were defined using high resolution electron beam lithography to reduce lithographically defined sidewall roughness. The lateral leakage current in a device consists of the spreading of current in the conductive upper cladding layer above the active region and the lateral out-diffusion of carriers in the active region.[17,25] In order to study only the effect of lateral leakage from out-diffusion on device performance, current spreading in the conductive upper cladding layer was eliminated by etching the ridge mesas down to the interface between the doped upper cladding layer and the undoped $GaAs-Al_{0.4}Ga_{0.6}As$ waveguide layer.[9,26–28] Etching was done using Cl_2/Ar inductively coupled plasma. The etched areas were planarised and insulated using Benzocyclobutene (BCB). AuGe/Ni/Au for n-type and AuZn for p-type metallization was used throughout.

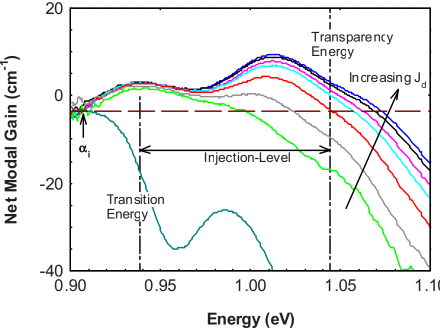

FIG. 1. (Color online) Measured TE net modal gain spectra for a 6 μm ridge at 350 K for a range of current densities. The modal loss spectrum is also shown. The horizontal dashed line marks the value of α_i, obtained from where the spectra converge at low energy. The vertical dashed lines indicate the transition energy (E_{trans}) and the transparency energy (ΔE_f) for the 556 A cm^{-2} gain curve (shown in bold). The injection-level at a 556 A cm^{-2} drive current is given by the difference between ΔE_f and E_{trans}.

The as-cleaved nonlasing multisection ridge test-structures were mounted p-side up onto copper blocks using silver epoxy for temperature controlled characterization by the SCM. The SCM is an electrical adaptation of the well-known single pass optical stripe length method. Through measurements of the single-pass amplified spontaneous emission as a function of pumped stripe length, the method allows us to determine the internal optical mode loss (α_i), the modal gain spectra (G), the modal absorption spectrum (A), the quasi-Fermi-level separation (ΔE_f), the unamplified spontaneous emission rate spectra (I_{sp}), the total intrinsic radiative current density (J_{rad}), and nonradiative current density (J_{nr}), and the overall internal quantum efficiency (η_{int}), as described in Ref. 11.

In the analysis, the actual values of the ridge widths were measured by scanning electron microscopy. All electrical device measurements were performed under pulsed conditions, with a pulse length of 500 ns at a frequency of 5 kHz (0.25% duty cycle) to avoid self-heating effects. Measurements of the TE polarized amplified spontaneous emission (TM emission was negligibly small) were recorded by a calibrated InGaAs camera array. Near-field measurements showed no filamentation in the devices, suggesting uniform distribution of the current across the mesa.

III. EXPERIMENTAL RESULTS AND DISCUSSION

An example of the TE net modal gain spectra ($G-\alpha_i$) obtained by a 6 μm ridge at 350 K is plotted as a function of photon energy for a range of drive current densities in Fig. 1. The net modal loss spectrum ($A+\alpha_i$) is also included for comparison. There are two distinct energy transitions observed in the net modal gain spectra which correspond to the inhomogenously broadened ground state (centered at

Downloaded 02 Apr 2012 to 131.251.133.28. Redistribution subject to AIP license or copyright; see http://jap.aip.org/about/rights_and_permissions

TABLE I. Measured values of the internal optical loss (α_i) and transition energy (E_{trans}) for a 10, 6, and 4 μm ridge at 350 K.

W (μm)	10	6	4
α_i (cm^{-1})	2.6 ± 0.7	3.4 ± 0.9	5.9 ± 0.6
E_{trans} (meV)	939.4 ± 1.1	940.0 ± 1.8	938.7 ± 1.2

~0.938 eV) and first excited state (centered at ~1.012 eV). The presence of a second excited state transition starts becoming apparent at higher drive current densities. At the low photon energy region, where there is zero optical gain and zero absorption, the gain and loss spectra converge together giving the value of the internal optical loss, α_i.[11,29] The transparency energy (ΔE_f) for a given drive current density can be identified from the point where the gain spectrum crosses the α_i value at high photon energy. Here the modal gain is zero and the energy equates to the quasi-Fermi-level separation for a system in quasithermal equilibrium. From the loss curve the transition energy (E_{trans}) of the material system is defined as the point where the absorption is half of the peak ground state absorption. Values for E_{trans} taken from the modal absorption spectrum of each ridge width are given in Table I. Within experimental error no variation with ridge width is seen and this is expected because the material system is the same. In the spirit of the Bernard and Durrafourg condition,[30] the quasi-Fermi-level separation relative to the "reference" transition energy, $\Delta E_f - E_{trans}$, is a measure of the intrinsic carrier injection-level for a given drive current density (i.e., a relative measure of the degree of population inversion). We therefore use this measurement to determine an intrinsic common operating point at which we can directly compare the performance of the different ridge widths.

Using the measured net modal gain spectra of each width device, we can analyze changes in the threshold current density with W by comparing the peak net modal gain characteristics as a function of drive current density; Fig. 2(a). This comparison shows that for a given net threshold gain ($G-\alpha_i$) condition, a higher nominal drive current density is needed as the ridge width is reduced from 10 to 4 μm. To exemplify this increase, Fig. 2(b) plots the drive current density required for a net modal gain of 4.7 cm^{-1}, which is the gain required to overcome the losses in a 2.7 mm long laser with mirror reflectivity 0.28.

There are fundamental mechanisms which can cause the apparent increase in threshold current density in the narrower ridges. These are: (1) an increasing internal optical loss, (2) a deteriorating gain-mode overlap, and (3) an increasing loss of carriers to lateral out-diffusion. For the purpose of this study we are primarily interested in the contribution from lateral out-diffusion. To separate this out we evaluate the relative impact of each mechanism.

A summary of the measurements of α_i, from data as plotted in Fig. 1 for each of the ridge widths, is given in Table I. We find that as the ridge width narrows from 10 μm the internal optical loss for the 6 and 4 μm ridges increases by a factor of 1.3 and 2.3, respectively. This effect can be largely attributed to an increase in scattering from the interaction of the optical mode with the roughness of the etched ridge.[12,13,31] In order to remove the effect of α_i on the threshold dependence with W we evaluate the modal gain, G, characteristics of each ridge width from the measured net modal gain ($G-\alpha_i$). In Fig. 3 the peak modal gain as a function of drive current density for each ridge width is given. The ground state peak modal gain shows little apparent dependence because over this drive current density range the gain varies gradually as it nears saturation. Had the increase in α_i been the only mechanism involved in the threshold dependence then the same excited state modal gain would have been exhibited by each ridge width for a given drive current density. To evaluate the contribution from the other two mechanisms, we can analyze the radiative current density, nonradiative current density, and modal gain in each ridge width as a function of intrinsic carrier injection-level ($\Delta E_f - E_{trans}$).

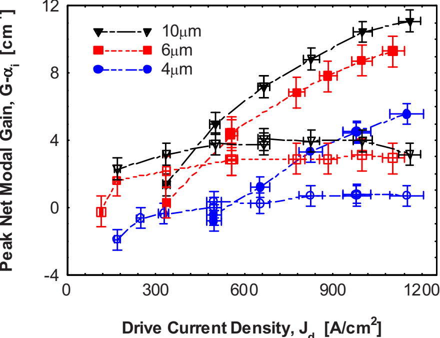

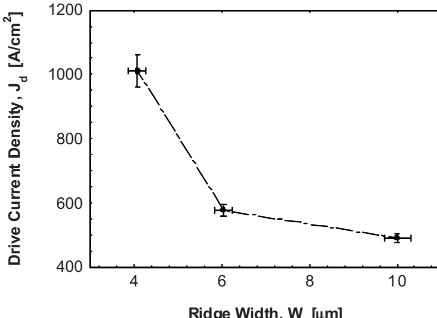

FIG. 2. (Color online) (a). The peak net modal gain ($G-\alpha_i$) as a function of drive current density for the ground (open symbols) and excited state (solid symbols) at 350 K. The black triangles, red squares, and blue circles correspond to the 10, 6, and 4 μm ridge widths. (b) The drive current density required for each ridge width to achieve a net modal gain of 4.7 cm^{-1} at 350 K. The graph is representative of the $J_{th}-W$ characteristic for 2.7 mm long shallow-etched ridge lasers with uncoated facets.

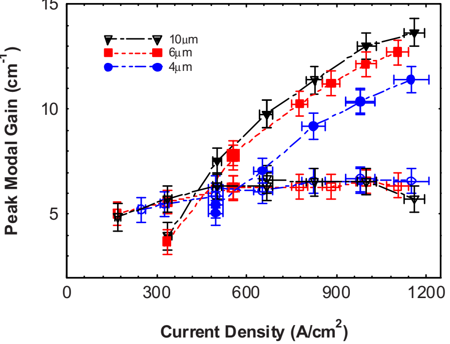

FIG. 3. (Color online) The peak modal gain (g) as a function of drive current density for the ground (open symbols) and excited state transitions (solid symbols) at 350 K.

Downloaded 02 Apr 2012 to 131.251.133.28. Redistribution subject to AIP license or copyright; see http://jap.aip.org/about/rights_and_permissions

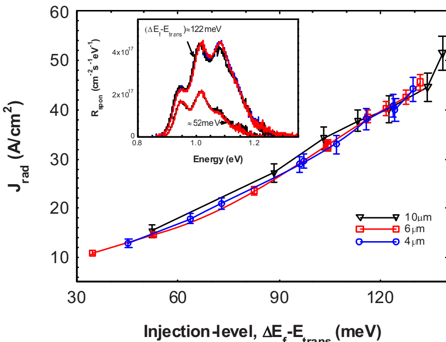

FIG. 4. (Color online) The total radiative current density (J_{rad}) as a function of injection-level ($\Delta E_f - E_{trans}$) for the 10, 6, and 4 μm ridges at 350 K. Inset: spontaneous emission rate spectra of the 10, 6, and 4 μm ridges at injection-levels in the region of 52 and 122 meV.

From the SCM, we can derive the unamplified spontaneous emission rate spectra from the amplified spontaneous emission (ASE) measurements.[11] This allows the total intrinsic radiative current density (J_{rad}) in the ridges to be determined by summing the integrated spontaneous emission rate spectra for each polarization and multiplying by the electronic charge. In Fig. 4, J_{rad} is plotted versus the intrinsic carrier injection-level ($\Delta E_f - E_{trans}$). This indicates that irrespective of ridge width the same average radiative current density is obtained for a common carrier injection-level ($\Delta E_f - E_{trans}$) and verifies the validity of defining an intrinsic common operating point for the range of ridge widths studied here. The spontaneous emission rate spectra used to derive this data are shown in the inset of Fig. 4 and confirm the similarity in spontaneous recombination rate is over the entire spectrum. We note that carriers diffusing outside of the spatial region described by the extent of the optical mode do not contribute to the radiative current density observed in the experiment and such recombination is classed as nonradiative current density in what follows.

Having determined that the different ridge widths are exhibiting the same radiative current density at a common injection-level, we can now examine the modal gain behavior with injection-level (Fig. 5) and evaluate any change in the gain-mode overlap.

A reduction in the gain-mode overlap, and hence modal gain, can be the effect of a change in the optical confinement factor (Γ) (Refs. 14–16) and/or a change in the lateral gain profile across the optical mode. Often in modeling the modal gain as a function of ridge width only the change in optical confinement is considered by evaluating $G = \Gamma g$, where g is the material gain and is assumed constant across the optical mode. Such an assumption for the bound fundamental mode within the ridge, and where the transverse optical confinement factor is calculated for the modal dot height (see e.g., Ref. 23 for the dot height distribution), yields a material gain estimate of 4×10^5 cm^{-1} at 330 A cm^{-2}. However, in real devices it may not be suitable to assume a spatially invariant g. Lateral out-diffusion or similarly surface recombination may strongly alter the carrier density profile across the lateral extent of the ridge and hence cause a nonuniform gain profile. In such situations, a change in G with ridge width is the result of changes in both the optical mode and material gain profile.[26,32] In Fig. 5, comparison of the peak modal gain behavior with intrinsic carrier injection-level shows a negligible difference between the different ridge widths. This implies that over the range of ridge width of 10 to 4 μm, the gain-mode overlap has not deteriorated significantly. The data in the inset shows the similarity of the modal gain over the entire spectrum. Syllogistically from Fig. 4, we can also deduce that the same radiative current density is required by the different ridge widths to produce the same modal gain. For sufficiently broad ridges this is expected behavior as the optical field profile[15] and gain producing lateral carrier density profile[10] change negligibly with ridge width. However for ridge widths somewhat narrower than those studied here, it is likely that the overlap between the optical field profile and the material gain distribution will deteriorate significantly. In this case, a lower modal gain will result when operating at the same carrier injection-level and concomitant radiative current density as that of a broader ridge. In order to then achieve the same modal gain, a higher gain-producing carrier density average, and concomitant radiative current density across the lateral extent of the mode would be required. This would be seen by an elevated carrier injection-level.

Having established that a deteriorating gain-mode overlap is not having a significant impact, we can reasonably deduce that the differences seen in Fig. 3 are from the lateral out-diffusion effect. To demonstrate this more clearly we compare the carrier injection-level achieved by each ridge width as a function of drive current density in Fig. 6. The narrower ridge widths are being pumped to a lower injection-level when operated with the same nominal drive current density. This is further illustrated in Fig. 7 where we see that the gain spectrum for nominally the same J_d within error of 980 A cm^{-2} becomes narrower and the transparency energy lower as the ridge width is reduced from 10 to 4 μm. Such behavior is typical of the expected increase in lateral out-diffusion effect, whereby a larger fraction of carriers are not pumping the active region but instead laterally diffusing and recombining outside of the gain region beneath the ridge. This is further supported by the data of Fig. 8 where we plot the nonradiative current density characteristic versus injection-level. We observe a higher nonradiative current

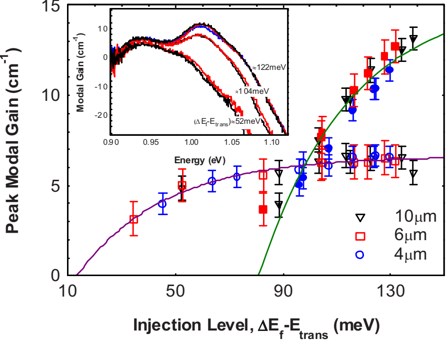

FIG. 5. (Color online) The peak modal gain as a function of carrier injection-level for the ground state (open symbols) and excited state (solid symbols) transitions at 350 K. Inset: modal gain spectra of the 10 (black) and 6 μm (red) ridges at injection-levels of approximately 52, 104, and 122 meV. The 4 μm (blue) ridge at approximately 122 meV is also shown.

Downloaded 02 Apr 2012 to 131.251.133.28. Redistribution subject to AIP license or copyright; see http://jap.aip.org/about/rights_and_permissions

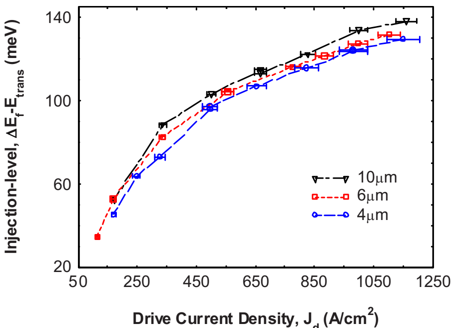

FIG. 6. (Color online) Carrier injection level ($\Delta E_f - E_{\rm trans}$) as a function of drive current density (J_d) for the 10 μm (black triangles), 6 μm (red squares), and 4 μm (blue circles) at 350 K.

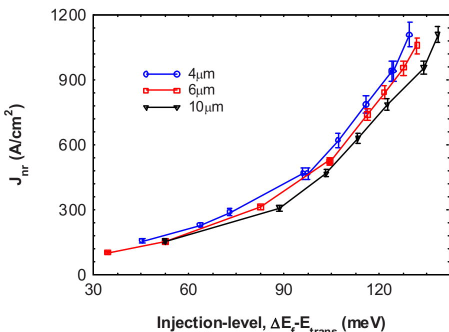

FIG. 8. (Color online) Nonradiative current density ($J_{\rm nr}$) associated with the 10 μm (black triangles), 6 μm (red squares), and 4 μm (blue circles) width ridges as a function of carrier injection-level ($\Delta E_f - E_{\rm trans}$), at 350 K.

density in the narrower ridge widths for a given injection-level, which is once more consistent with an increasingly larger fraction of injected carriers being lost to lateral out-diffusion with decreasing ridge width. The data of Fig. 6, which suggests that a larger drive current density is required at smaller W to obtain the same injection-level, is therefore taken to be the result of the increasing fraction of lateral out-diffusion loss. This dependence is illustrated in Fig. 9 for an injection-level of 122 and 53 meV. These injection-levels correspond to a threshold modal gain of 10.8 cm^{-1} for 1.2 mm lasers, and 4.7 cm^{-1} for 2.7 mm lasers, respectively.

The fractional increase in drive current density at an injection-level of 122 meV for the 6 and 4 μm ridges with respect to the 10 μm ridge is 1.07 and 1.14, respectively. Since this is a fairly small impact it implies that the lateral ambipolar diffusion length will also be fairly small. In Sec. IV a standard ambipolar diffusion model will be used to fit the increase in drive current density that is caused by lateral out-diffusion to establish the lateral ambipolar diffusion length at various carrier injection-levels.

IV. AMBIPOLAR DIFFUSION LENGTH ANALYSIS

Having separated the threshold dependence on ridge width due to the mechanism of lateral out-diffusion only, we can now fit the data with a standard diffusion length model and establish the ambipolar diffusion length at various carrier injection-levels. The model requires analytically solving the steady-state ambipolar diffusion equation to obtain the lateral carrier density profile. The mechanics of doing this have been described elsewhere, notably in Refs. 9, 10, and 17. In this analysis we adapt the approach of Letal.[10]

A. Lateral out-diffusion modeling

In the single pass, SCM experiment where stimulated emission is negligible, the steady-state ambipolar diffusion equation of the lateral carrier density profile is given by

$$D_a \frac{\partial^2 n(x)}{\partial x^2} + \frac{J_d}{d \cdot q} - \frac{n(x)}{\tau} = 0, \quad (1)$$

where $n(x)$, τ, d, J_d, D_a denote the carrier density profile in the lateral direction, average carrier lifetime, active region thickness, drive current density, and effective ambipolar diffusion coefficient, respectively. In the construction of (1), the carrier density profile is taken to be uniform across the thickness of the active region. This essentially simplifies what would otherwise be a two-dimensional problem into a one-dimensional problem along the lateral direction.

Equation (1) is solved analytically by considering a high injection-level regime with the following simplifications. Under high injection conditions the excess carrier concentrations are much greater than the intrinsic thermal equilibrium carrier concentration. The condition of quasicharge neutrality is maintained as the active region is undoped.[33] For the device structure used, the area of current injection into the active region is limited by the boundaries of ridge at $x = \pm W/2$. This injected drive current density, J_d, is assumed to be uniform across W and zero elsewhere (i.e., a step function). An illustration of the modeled ridge and parameters are

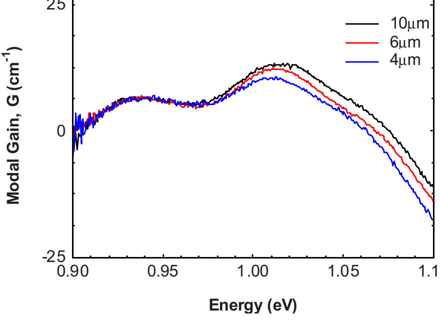

FIG. 7. (Color online) Modal gain (g) spectra for the 10 (black), 6 (red), and 4 μm (blue) devices at a J_d, within error, of 980 A cm^{-2}.

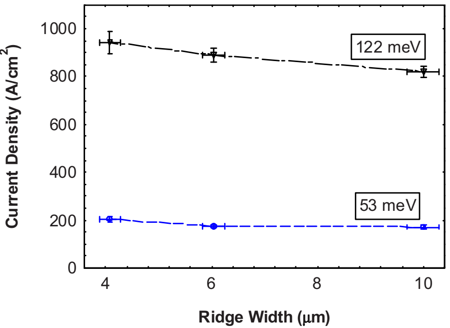

FIG. 9. (Color online) Dependence of J_d on ridge width at common injection-levels of 122 (solid) and 53 meV (open).

Downloaded 02 Apr 2012 to 131.251.133.28. Redistribution subject to AIP license or copyright; see http://jap.aip.org/about/rights_and_permissions

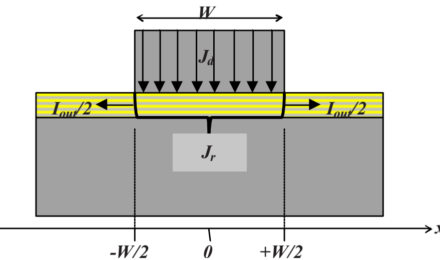

FIG. 10. (Color online) Illustration of the current paths used in Eq. (2) and the coordinate system of the carrier diffusion model.

given in Fig. 10. This figure also illustrates the average recombination current density beneath the ridge, J_r, and the total lateral out-diffusion current that occurs from the recombination of carriers diffusing out of the active region beneath the ridge, I_{out}.

Taking the carrier lifetime (τ) to be spatially invariant, Eq. (1) is solved by matching the continuity of current $[dn(x)/dx]$ and carrier concentration $[n(x)]$ at the ridge boundary. This yields the lateral carrier density profile both inside Eq. (2a) and outside Eq. (2b) of the ridge

$$n(x) = \frac{J_d \cdot \tau}{q \cdot d}\left(1 - e^{-W/2L_d} \cdot \cosh\left(\frac{x}{L_d}\right)\right), \quad |x| \leq \frac{W}{2}, \tag{2a}$$

$$n(x) = \frac{J_d \cdot \tau}{q \cdot d} e^{-|x|/L_d} \cdot \sinh\left(\frac{W}{2L_d}\right), \quad |x| \geq \frac{W}{2}, \tag{2b}$$

where the lateral ambipolar diffusion length, L_d, is given by $\sqrt{D_a \tau}$. We can now determine the average recombination current density beneath the ridge by integrating laterally over the width of the ridge according to

$$J_r = \frac{d \cdot q}{W} \int_{-w/2}^{w/2} \frac{n(x)}{\tau} dx, \tag{3}$$

to yield

$$J_r = J_d\left(1 - \frac{L_d}{W}(1 - e^{-W/L_d})\right). \tag{4}$$

In the study by Letal,[10] the average recombination beneath the ridge was assumed to be independent of ridge width at a common operation point such as threshold. In our application of the model we will make the same assumption but at a more restrictively defined common operating point: that of a common intrinsic carrier injection-level. In Sec. III, we proved this to be a suitable assumption through our experimental results on the spontaneous emission and radiative recombination current density. These measurements collectively showed that the radiative recombination current density was independent of ridge width for a given injection-level. It is therefore reasonable to assume that J_r is the same in all ridge widths at a common injection-level.

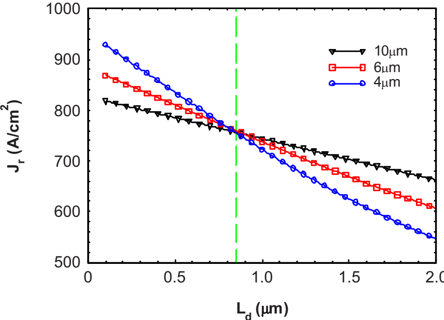

FIG. 11. (Color online) The $J_r - L_d$ relation for the 10 (black triangles), 6 (red squares), and 4 μm (blue circles) ridges at an injection-level of 122 meV and temperature of 350 K. The intercept of all three relations gives the lateral ambipolar diffusion length to be 0.84 μm.

TABLE II. Values for the measured W, J_d, J_{rad}, J_{nr} at an injection-level of 122 meV and the calculated J_r using a L_d of 0.84 μm.

W (μm)	J_d (A cm^{-2})	J_{rad} (A cm^{-2})	J_{nr} (A cm^{-2})	J_r (A cm^{-2})
4.08	952.00	40.38	912.00	757.52
6.04	883.00	40.26	842.74	760.29
10.00	826.67	40.16	786.51	757.23

With the above boundary condition we can now use a simple fitting routine to determine J_r and L_d, without the need to model the gain profile and subsequently calculate a threshold point from what can be inappropriate parameters and relations to broad area devices. The routine involves plotting the function J_r with respect to L_d for each ridge width by using Eq. (4) and the measured drive current density values for operation at a particular injection-level. The boundary condition of a common J_r leads to the ambipolar diffusion length as shown in Fig. 11, which is an example for an injection-level of 122 meV. The plot illustrates that only one solution for L_d exists for a common J_r, which for this case is an L_d and J_r of approximately 0.84 μm and 759 A cm^{-2}, respectively. In Table II, the calculated parameters of J_r for a L_d of 0.84 μm are given along with the measured parameters for W, J_d, J_{rad}, and J_{nr} at an injection-level of 122 meV.

In Fig. 12, the modeled $J_d - W$ relation for an L_d of 0.84 μm and J_r of 759 A cm^{-2} is given, along with the measured $J_d - W$ relation at an injection-level of 122 meV. In comparing the theoretical and experimental plot, it is clearly evident that the carrier diffusion model accurately explains the measured increase in threshold current density with decreasing ridge width and in doing so yields a good assessment of the lateral ambipolar diffusion length. The theoretical plot also shows the typical behavior seen in very wide ridge widths: where the threshold current density changes

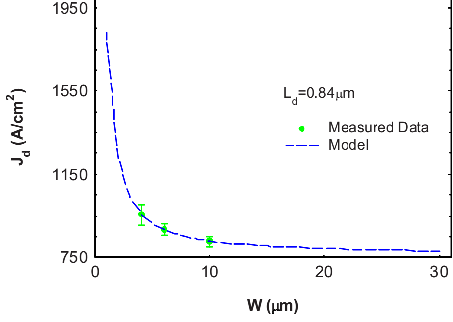

FIG. 12. (Color online) The calculated $J_d - W$ relation for a L_d of 0.84 μm, along with the measured $J_d - W$ relation at an injection-level of 122 meV.

Downloaded 02 Apr 2012 to 131.251.133.28. Redistribution subject to AIP license or copyright; see http://jap.aip.org/about/rights_and_permissions

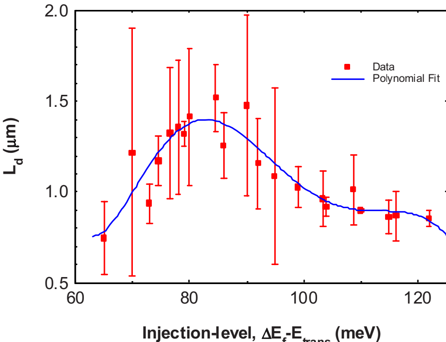

FIG. 13. (Color online) Estimated lateral ambipolar diffusion length (L_d) as a function of injection-level ($\Delta E_f - E_{trans}$) in the quantum-dot active region at 350 K.

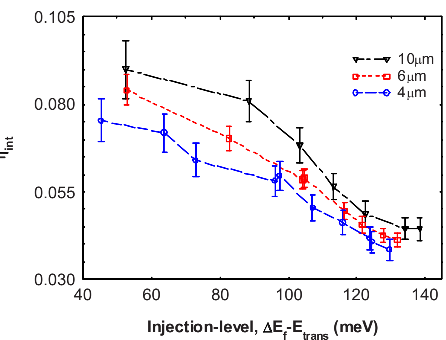

FIG. 14. (Color online) Internal quantum efficiency (η_{int}) as a function of carrier-injection-level for the 10 (black triangles), 6 (red squares), and 4 μm (blue circles) ridges at 350 K.

negligibly with ridge width when L_d is much smaller than the W. Here the out-diffusion loss is a very weak function of ridge width and can be approximated to a constant.

B. L_d dependence on injection-level

In the above analysis L_d was determined for an injection-level (122 meV) which corresponded to a threshold modal gain of 10.8 cm^{-1} and cavity length of 1.2 mm. By performing the same analysis at other injection-levels it has been possible to determine L_d as a characteristic of how hard a device is being pumped. This characteristic is useful for understanding the mechanism of lateral carrier diffusion in the coupled QD/wetting-layer/barrier system. The results of this analysis are presented in Fig. 13, where L_d was determined over a range of injection-levels covering 65 to 122 meV by means of interpolation between data points of the injected drive current density. The peak modal gain exhibited over this range is approximately from 5 to 11 cm^{-1} as given by Fig. 5. The error in L_d in Fig. 13 comes from the range of values which satisfy a common J_r and best fit the measured data. The error varies in accordance to the extent of interpolation between measured data points; with the smallest errors coinciding with closely matched data points.

The general trend of the L_d —*injection-level* characteristic seen in Fig. 13 has two distinct regions.

- The first region is at low injection-levels where L_d appears to be increasing with increasing injection-level. The increase in L_d is approximately from 0.75 to 1.5 μm over an injection-level range of 65–84 meV.
- At higher injection-levels there is an apparent decrease in the lateral ambipolar diffusion length. The decrease is approximately from 1.5 to 0.85 μm over the injection-level range of 84–122 meV.

The increase in L_d with carrier injection-level is somewhat intuitive and can be explained as follows. As the device is driven harder, the quasi-Fermi-level separation increases and the higher energy states of the quantum-dots get increasingly populated. Carriers in the excited states of the quantum-dots experience a smaller confining potential than those in lower states (carriers in the ground state will experience the highest confining potential) and when this confining potential is comparable to the thermal energy of the system, thermally assisted excitation into the wetting-layer can more readily occur. Once in the wetting-layer, carriers no longer experience a lateral confinement and are able to diffuse laterally along the two dimensions of the QW plane before recombining or being captured into another dot. This process thereby increases the apparent lateral ambipolar diffusion length of carriers in the active region system as a whole.

In contrast the decrease in the lateral ambipolar diffusion length is an unexpected result. What follows is a discussion with supportive analysis to a plausible explanation that is consistent with the overall experimental findings.

With the increase in population of the quantum-dot excited states and wetting-layer with injection-level, there seems be a mechanism which has the effect of reducing the average carrier lifetime and hence the apparent lateral ambipolar diffusion length of the system. It could be a nonradiative recombination process such as Auger becoming significant at higher carrier densities in the QD excited states and/or wetting layer. Indeed, the nonradiative current density measurements in Fig. 8 do have a higher order increase after a carrier injection-level of 84 meV. Moreover, by determining the internal quantum efficiency ($\eta_{int}=J_{rad}/J_d$) as a function of carrier injection-level, as illustrated in Fig. 14, it can be seen that below about 84 meV, η_{int} gradually decreases with increasing injection-level for all of the ridge widths. The 10 μm ridge is the most efficient as expected since it has the least fraction of lateral out-diffusion current. At the highest injection levels the internal efficiencies for different ridge widths converge.

The initial gradual decrease in η_{int} coincides with the region where L_d is seen to increase with injection-level. Presumably this behavior is primarily caused by the increasing thermal re-emission into the wetting-layer with increasing injection-level. This process continues at higher injection-levels, but the increasing number of carriers in the quantum-well like wetting-layer gives rise to a higher nonradiative recombination rate. The effect of this reduces the average carrier lifetime in the wetting layer and concomitantly the ambipolar diffusion length. This process seems dominant in this regime, such that the lower carrier lifetime reduces the relative effect of carrier out-diffusion, as observed by the reduced difference in η_{int} between the different ridge widths, to produce a smaller L_d.

Downloaded 02 Apr 2012 to 131.251.133.28. Redistribution subject to AIP license or copyright; see http://jap.aip.org/about/rights_and_permissions

In a QW, Auger recombination has an approximate cubic relation to the carrier density and therefore as the population in the wetting-layer increases, the rate of Auger recombination may also increase and cause the average carrier lifetime to decrease. Such behavior has been observed in a standard quantum-well structure where increasing the injection-level was observed to rapidly decrease the carrier lifetime as a result of higher order nonradiative processes.[34] In the report by Ongstad,[34] the carrier lifetime was observed to decrease rapidly with carrier injection-level and eventually saturate. This saturation phenomenon is caused by band filling and the eventual population of the barrier states where carriers recombine more readily by monomolecular processes. Filling of the barrier states with increased injection effectively saturates the population of the quantum-well and thereby the higher order recombination rate with increased injection. A similar process involving the surrounding barrier material may be observed in our measurements as L_d is observed to level-off to an approximately fixed value of 0.84 μm (Fig. 13). Recognition of such behavior implies that the observed reduction in L_d at higher injection level in this study is because the population of carriers in the QW wetting-layer has reached a point where any further increase in population results in a decrease in the average carrier lifetime and hence diffusion length.

We note that the single pass amplified spontaneous emission experiments performed here accurately predict the behavior of lasers up to threshold, where stimulated emission has a relatively small contribution, but do not include all the effects of a reducing stimulated emission lifetime that may be important significantly above threshold. Such a reduction in lifetime would also lead to some reduction in the apparent ambipolar diffusion length in a laser significantly above threshold. From this analysis we can conclude that the expected reduction in L_d as a result of three-dimensional carrier confinement in quantum-dot material systems only occurs at threshold conditions that require low carrier injection-levels. At higher threshold carrier injection-levels it is the increased nonradiative recombination rate that predominantly reduces L_d.

C. Temperature dependence

Given that thermal re-emission from the quantum-dot to the wetting layer-energy ought to increase with increasing temperature, it would be reasonable to assume that decreasing the temperature will reduce the thermal re-emission and thereby L_d. In such a case fewer carriers will be escaping into the wetting layer where lateral diffusion can occur. In Fig. 15 we show the nonradiative current density as a function of injection-level for the various ridge widths at 300 K.

Within the experimental uncertainty the difference between the nonradiative current density in the different ridge widths is negligible at injection-levels below 121 meV. Correspondingly the injection-level is independent of ridge width for a given drive current density over this range (inset of Fig. 14). This implies that at 300 K the loss of carriers to lateral out-diffusion is approximately the same in the different widths within this range. This behavior is consistent with

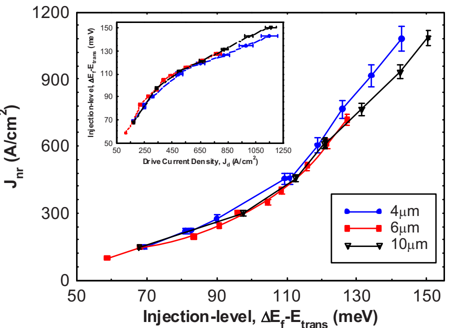

FIG. 15. (Color online) Nonradiative current density for the 10, 6, and 4 μm ridges as a function of injection-level, at 300 K. Inset: corresponding carrier injection level as a function of drive current density for the 10, 6, and 4 μm at 300 K.

a lateral ambipolar diffusion length that is much smaller than the ridge width. Given that at 350 K a difference in nonradiative current density in the different ridge widths was observable for an ambipolar diffusion length of 0.75 μm, it therefore seems that the lateral ambipolar diffusion length must be less than 0.75 μm at 300 K for injection-levels below 121 meV. The reduced thermal re-emission at lower temperatures and low injection levels does thereby reduce the lateral ambipolar diffusion length.

At injection-levels above 121 meV the nonradiative recombination current density in the 4 μm ridge starts to become higher than the 10 μm ridge and this is consistent with the increased population of the wetting layer at the highest injection-levels. The resulting onset of a significant lateral out-diffusion effect now causes a lower injection-level for the 4 μm ridge in comparison to the 10 μm at a given drive current density. The threshold current density will therefore increase for any fixed value of modal gain.

V. DISCUSSION

There are several reasons why it is difficult to relate the values of L_d in the InAs quantum-dot-in-a-well material system obtained in this investigation at various carrier injection-levels (L_d=0.75–1.50 μm) to those reported in the literature.

- First the material system is not exactly the same,
- second the measurements are not necessarily at the same temperature,
- third the measurements would have almost certainly been taken at different injected carrier densities,
- and lastly changes in α_i and gain-mode overlap are not completely accounted for in the previous studies.

Nonetheless it is useful to see where the obtained values of L_d in this study lie in the range of reported values.

Using the $J_{th}-W$ characteristic of InAs quantum-dots-in-a-well ridge lasers (emitting at 1280 nm) and device modeling that includes solving the ambipolar diffusion equation, Moore *et al.*[8] found L_d to be 1.0 μm at an unstated temperature. Other studies on self-assembled quantum-dots found lateral ambipolar diffusion length values of $L_d \sim 6.5$ μm (Ref. 6) (using a spatially resolved microphotoluminescence technique at room temperature on InAs QDs emitting at

Downloaded 02 Apr 2012 to 131.251.133.28. Redistribution subject to AIP license or copyright; see http://jap.aip.org/about/rights_and_permissions

~1120 nm), $L_d \sim 1.65$ μm (Ref. 35) (using spatially resolved photoluminescence at room temperature on InAs quantum-dots-in-a-well emitting at 1270 nm), $L_d \sim 0.5$ μm (Ref. 36) (using a cathodoluminescence technique at room temperature on $In_{0.3}Ga_{0.7}As$ QDs emitting at 1180 nm), and $L_d < 100$ nm (Ref. 7) (obtained by analyzing the scaling behavior of the I-V and L-I characteristics in an InAs quantum-dot system emitting around 1300 nm at room temperature). In general the obtained values of L_d in this study are not that dissimilar to the previously reported values of similar structures. However, in this investigation we have ensured that the mechanisms of an increasing internal optical loss and deteriorating gain-mode overlap are not influencing the estimate. Most significantly our measurements also show how L_d can differ considerably depending on the carrier injection-level, and this in itself may also contribute to the variation in values reported in the different studies.

Our study suggests that the overall diffusion mechanism is the result of thermally assisted redistribution via the wetting-layer. But in addition it reveals that at high enough carrier injection-levels, higher-order nonradiative processes reduce the average carrier lifetime and consequently the observed lateral ambipolar diffusion length. This is not a change in the mechanism but rather a change in a key parameter which governs it. This shows that when assessing the performance of quantum-dot devices, either in terms of scaling or comparatively with other material systems, care should be taken in attributing any empirical signs of a reduced ambipolar diffusion length to purely improved carrier localization and greater energy discontinuity between the wetting-layer states. It also throws some further light on the origin of the poor temperature dependence of threshold current observed in some quantum dot lasers at the very highest temperatures,[37] suggesting significant recombination may be occurring in the wetting layer.

To reduce the lateral out-diffusion mechanism while maintaining radiative efficiency, to either allow further miniaturization or integration of deep-etched features, it is necessary to optimize for operation on the ground state. This will require the following.

- Low internal optical loss. However, from the measurements on the internal optical loss, this may not be possible as α_i was found to increase significantly with reducing the ridge width. This effect will increase the threshold gain requirement and may cause lasing on the higher-energy states where there is more gain. Lasing on a higher energy state will increase the lateral ambipolar diffusion length as carriers populating the higher energy states require less energy to thermally escape into the wetting layer and diffuse.
- Higher ground state modal gain. This may be possible by increasing the number of quantum-dot layers, reducing the inhomogeneous broadening or increasing the QD density. The increased number of states at a given energy will result in a lower injection-level for a given threshold modal gain. Assuming that the QD separation remains sufficiently large, so that tunneling effects are negligible, and that the defect density is unchanged such devices would then operate with a lower ambipolar diffusion length at threshold. However, we would expect the ambipolar diffusion length measured as a function of injection-level, as described in this paper, would not be significantly different.

VI. CONCLUSIONS

In summary, we have used the SCM on different ridge width devices to evaluate the threshold dependence on ridge width. The analysis allowed the separation and numerical evaluation of the components making up the threshold dependence, i.e., an increasing internal optical loss, a deteriorating gain-mode overlap, and an increasing lateral out-diffusion loss. Separating the contribution from lateral out-diffusion, allowed us to determine L_d by fitting the data with a standard ambipolar diffusion length model. Further analysis then allowed us to determine the behavior of L_d with intrinsic carrier injection-level. At 350 K L_d was found to range from 0.75–1.50 μm over an injection-level range of 65–122 meV. Reducing the temperature to 300 K resulted in a lower L_d of <0.75 μm for injection-levels below 121 meV. Significantly, two distinct regimes of operation were revealed where the ambipolar diffusion length can be reduced. The beneficial regime, in terms of device performance, is at low injection-levels where carriers populate the lower states of the dots. The other regime is at high injection-levels, where the average carrier lifetime and concomitantly L_d reduces with the increased population of the wetting-layer. This latter effect is probably caused by higher order nonradiative processes. This observation highlights that improvements in device miniaturization and integration with deep-etched features can be made by optimizing device operation for the low injection-level regime. The findings are consistent with the mechanism of lateral diffusion in the coupled system of quantum-dots/wetting-layer/barrier involving the thermal redistribution of carriers via the wetting-layer and may partly explain the large variations in the previously reported values for the diffusion length in quantum dot materials.

ACKNOWLEDGMENTS

The authors acknowledge the financial support of the UK EPSRC under Grant No. EP/F006683. We would also like to thank Professor P. Blood and Dr. M. Mexis for their helpful discussions, Professor Mark Hopkinson and Dr. Hui-yun Liu for sample growth, and Dr. A. Sobiesierski for her help in device fabrication.

[1] D. Bimberg, M. Grundmann, and N. N. Ledentsov, *Quantum Dot Heterostructures* (Wiley, Chichester, 1999).
[2] M. Sugawara, N. Hatori, M. Ishida, H. Ebe, Y. Arakawa, T. Akiyama, K. Otsubo, T. Yamamoto, and Y. Nakata, J. Phys. D: Appl. Phys. **38**, 2126 (2005).
[3] N. N. Ledentsov, M. V. Maximov, P. S. Kopev, V. M. Ustinov, M. V. Belousov, B. Y. Meltser, S. V. Ivanov, V. A. Shchukin, Z. L. Alferov, M. Grundmann, D. Bimberg, S. S. Ruvimov, W. Richter, P. Werner, U. Gosele, J. Heidenreich, P. D. Wang, and C. M. S Torres, Microelectron. J. **26**, 871 (1995).
[4] J. K. Kim, R. L. Naone, and L. A. Coldren, IEEE J. Sel. Top. Quantum Electron. **6**, 504 (2000).

Downloaded 02 Apr 2012 to 131.251.133.28. Redistribution subject to AIP license or copyright; see http://jap.aip.org/about/rights_and_permissions

[5]J. M. Gérard, O. Cabrol, and B. Sermage, Appl. Phys. Lett. **68**, 3123 (1996).
[6]A. Shaw, H. Folliot, and J. F. Donegan, Nanotechnology **14**, 571 (2003).
[7]A. Fiore, M. Rossetti, B. Alloing, C. Paranthoen, and J. X. Chen, Phys. Rev. B **70**, 205311 (2004).
[8]S. A. Moore, L. O'Faolain, M. A. Cataluna, M. B. Flynn, M. V. Kotlyar, and T. F. Krauss, IEEE Photon. Technol. Lett. **18**, 1861 (2006).
[9]S. Y. Hu, S. W. Corzine, K.-K. Law, D. B. Young, A. C. Gossard, L. A. Coldren, and J. L. Merz, J. Appl. Phys. **76**, 4479 (1994).
[10]G. J. Letal, J. G. Simmons, J. D. Evans, and G. P. Li, IEEE J. Quantum Electron. **34**, 512 (1998).
[11]P. Blood, G. M. Lewis, P. M. Smowton, H. Summers, J. Thompson, and J. Lutti, IEEE J. Sel. Top. Quantum Electron. **9**, 1275 (2003).
[12]K. K. Lee, D. R. Lim, H.-C. Luan, A. Agarwal, J. Foresi, and L. C. Kimerling, Appl. Phys. Lett. **77**, 1617 (2000).
[13]D. Liang, J. Wang, J.-T. Huang, J. Yeh, L. Mawst, and D. Hall, IEEE J. Sel. Top. Quantum Electron. **13**, 1324 (2007).
[14]E. Kapon, Opt. Lett. **15**, 801 (1990).
[15]J. S. Osinski, K. M. Dzurko, S. G. Hummel, and P. D. Dapkus, Appl. Phys. Lett. **56**, 2487 (1990).
[16]U. T. Schwarz, M. Pindl, E. Strum, M. Furitsch, A. Leber, S. Miller, A. Lell, and V. Härle, Phys. Status Solidi A **202**, 261 (2005).
[17]W. T. Tsang, J. Appl. Phys. **49**, 1031 (1978).
[18]S. Y. Hu, D. B. Young, A. C. Gossard, and L. A. Coldren, IEEE J. Quantum Electron. **30**, 2245 (1994).
[19]S. Evoy, G. F. Redinbo, and H. G. Craighead, Appl. Phys. Lett. **68**, 1259 (1996).
[20]V. Malyarchuk, J. W. Tomm, V. Talalaev, and C. Lienau, Appl. Phys. Lett. **81**, 346 (2002).
[21]R. J. Nelson, J. S. Williams, H. J. Leamy, B. Miller, H. C. Casey, Jr., B. A. Parkinson, and A. Heller, Appl. Phys. Lett. **36**, 76 (1980).
[22]W. S. Hobson, F. Ren, U. Mohideen, R. E. Slusher, and M. Lamont Schnoes, J. Vac. Sci. Technol. A **13**, 642 (1995).
[23]H. Y. Liu, I. R. Sellers, T. J. Badcock, D. J. Mowbray, M. S. Skolnick, K. M. Groom, M. Gutierrez, M. Hopkinson, J. S. Ng, and J. P. R. David, Appl. Phys. Lett. **85**, 704 (2004).
[24]H. Y. Liu, I. R. Sellers, M. Gutierrez, K. M. Groom, W. M. Soong, M. Hopkinson, J. P. R. David, R. Beanland, T. J. Badcock, and D. J. Mowbray, J. Appl. Phys. **96**, 1988 (2004).
[25]W. Joyce, J. Appl. Phys. **51**, 2394 (1980).
[26]G. Adolfsson, S. Wang, M. Sadeghi, J. Bengtsson, A. Larsson, J. J. Lim, V. Vilokkinen, and P. Melanen, IEEE J. Quantum Electron. **44**, 607 (2008).
[27]H. Wenzel, G. Erbert, A. Knauer, A. Oster, K. Vogel, and G. Trankle, Semicond. Sci. Technol. **15**, 557 (2000).
[28]C. Y. Liu, Y. Qu, S. Yuan, and S. F. Yoon, Appl. Phys. Lett. **85**, 4594 (2004).
[29]S. Inada, M. Yoshita, M. Okano, T. Ihara, H. Akiyama, and L. Zhang, Jpn. J. Appl. Phys. **47**, 2288 (2008).
[30]M. G. A. Bernard and G. Duraffourg, Phys. Status Solidi **1**, 699 (1961).
[31]R. K. Price, V. B. Verma, V. C. Elarde, and J. J. Coleman, J. Appl. Phys. **103**, 013108 (2008).
[32]L. A. Coldren and S. W. Corzine, *Diode Lasers and Photonic Integrated Circuits* (Wiley Series in Microwave and Optical Engineering, New York, 1995).
[33]T. Strand, B. Thibeault, and L. Coldren, J. Appl. Phys. **81**, 3377 (1997).
[34]A. P. Ongstad, D. J. Gallant, and G. C. Dente, Appl. Phys. Lett. **66**, 2730 (1995).
[35]D. P. Popescu, P. G. Eliseev, A. Stintz, and K. J. Malloy, J. Appl. Phys. **94**, 2454 (2003).
[36]J. K. Kim, T. A. Strand, R. L. Naone, and L. A. Coldren, Appl. Phys. Lett. **74**, 2752 (1999).
[37]P. M. Smowton, A. A. George, I. C. Sandall, M. Hopkinson, and H.-Y. Liu, IEEE J. Sel. Top. Quantum Electron. **14**, 1162 (2008).

Downloaded 02 Apr 2012 to 131.251.133.28. Redistribution subject to AIP license or copyright; see http://jap.aip.org/about/rights_and_permissions